Model of Anomalous Fluid Filtration in a One-Dimensional Homogeneous Porous Medium

KHUZHAYOROV B.[1,2], DZHIYANOV T.[1,3], AKRAMOV SH.[1]
[1] Department of Mathematical Modeling,
Faculty of Mathematics, Samarkand State University,
15, University Blvd., Samarkand 140104,
UZBEKISTAN

[2] Institute of Mathematics named after V.I. Romanovsky,
Academy of Sciences, Ruz, Tashkent,
UZBEKISTAN

[3]Kimyo International University in Tashkent,
UZBEKISTAN

Abstract: - In this paper, the anomalous filtration of a homogeneous fluid in a homogeneous porous medium is considered. A model of anomalous fluid filtration, composed using the fractional differentiation apparatus, is then numerically analyzed. Problems with constant, exponential, and sinusoidal boundary conditions are considered. The influence of the anomaly on the distribution of the pressure field and filtration velocity is estimated.

Key-Words: - Anomalous filtration, anomalous Darcy's law, filtration velocity, fractional derivative, one-dimensional, porous media.

Received: March 26, 2025. Revised: June 21, 2025. Accepted: July 23, 2025. Published: November 25, 2025.

1 Introduction

Darcy's law is commonly used to model fluid flow in porous media, particularly oil and gas. This law establishes a relationship between filtration velocity and pressure gradient. However, Darcy's law is not applicable in a number of cases, and studying oil recovery processes based on the classical Darcy's law does not lead to satisfactory results. Fluids typically carry solid particles with them as they move, and these particles can block some pores, leading to a decrease in porosity or even their closure. Over time, permeability decreases, the effect of the pressure gradient on fluid flow through the medium is delayed, and the flow occurs as if it had a memory, [1].

The proposed mathematical model in [2] is suitable for describing anomalous diffusion observed in media with fractal geometry, as well as in disordered and highly inhomogeneous porous media. A numerical scheme based on the existing discretization method is used to process the modified memory-based mathematical model. The accuracy of the numerical model is confirmed by an analytical solution of a simplified problem.

Various formulas describing non-Darcy flow have been used to quantify fluid flow in natural geological environments, but there is no universal law or formula that can reliably describe the complex relationship between flow velocity and pressure gradient for single-phase fluid flow in natural oil and gas reservoirs. Model fitting shows that the spatial fractional Darcy's law can accurately reflect the flow properties and agrees well with the experimental data presented in the seepage curves. The model parameters can also be significantly simplified to allow for a possible physical interpretation closely related to the structure of the medium, [3].

In [4], a larger number of laboratory experiments were conducted using different sand sizes and pressures to study how different conditions could affect the memory. In addition, the number of memory parameters was increased so that the calculations could quantitatively represent the asymptotic value of the flow. Good agreement was obtained between the time variations of both the theoretical and observed flow.

In [5], [6] a memory mechanism was presented that mathematically models possible changes in the physical properties of the matrix due to changes in its temperature and physical or chemical interaction with the fluid. The elastic response of the matrix is neglected, the diffusion equations are separated from the elasticity equations, which are not considered here, and the main attention is paid to the fluid pressure, which is periodically observed in the flow, as in the case of periodic boundary conditions. At first glance, it may seem that the introduction of mathematical memory into the formulation of the governing equations complicates the problem, however, the use of the Laplace transform (LT) allows one to obtain a solution directly under the given boundary conditions.

In [7] we consider an extension of the constitutive diffusion relation to the case when the space memory mechanism operates. The order of the medium is expressed by differential equations of fractional order covering the continuum in a given range, then the constitutive equation becomes a differential equation of distributed order.

In [8] homogeneous and heterogeneous media with different characteristic particle sizes were used. It was shown that the memory parameters, especially the low value assumed in terms of the decimal order, influence the experiment in many ways. The data and theory showed how mechanical compression can reduce the conductivity and hence the flow.

In this paper, based on the filtration law [9], which takes into account the effects of changing the permeability of the medium, the filtration equation with dependent on pressure is derived. For this equation, some problems in a finite layer are set, considered with different boundary conditions. The modes of constant, exponentially increasing, and harmonically changing pressure at one of the boundaries of the medium are considered. The fields of pressure and filtration velocity are determined for various values of the parameter α, characterizing the memory effects in the filtering law.

2 Derivation of the Filtration Equation

The law of anomalous filtration is taken as [9], [10], [11]:

$$\vec{\upsilon} = -\frac{k_f}{\mu}\nabla\left(\frac{\partial^\alpha p}{\partial t^\alpha}\right), \tag{1}$$

where is $\vec{\upsilon}$ – the filtration velocity, k_f is the pseudo-permeability, i.e. fractal permeability with the dimension L^2T^α, L is the dimension of length, T is the dimension of time, μ is the viscosity of the liquid, $\alpha(0<\alpha\le 1)$ is the order of the derivative, ∇ is the Hamilton operator, p is the pressure.

Let us take the continuity equation in the form [12], [13]:

$$\frac{\partial(\rho m)}{\partial t} + div\left[\rho\vec{\upsilon}\right] = 0, \tag{2}$$

where ρ is the density of the liquid $\left(\frac{kg}{m^3}\right)$, m is the porosity of the medium $\left(\frac{m^3}{m^3}\right)$

Substituting (1) into (2) we obtain

$$\frac{\partial(\rho m)}{\partial t} - div\left[\frac{k_f\rho}{\mu}\nabla\left(\frac{\partial^\alpha p}{\partial t^\alpha}\right)\right] = 0. \tag{3}$$

We assume that the skeleton of the porous medium and the liquid are compressible, and the viscosity of the liquid is constant. In addition, the medium is non-uniform in permeability, etc. k_f is a function of coordinates.

Let's transform the second term in (3) as:

$$\begin{aligned} div\left[\rho\nabla\left(\frac{\partial^\alpha p}{\partial t^\alpha}\right)\right] &= \rho\Delta\left(\frac{\partial^\alpha p}{\partial t^\alpha}\right) + \nabla\rho\cdot\nabla\left(\frac{\partial^\alpha p}{\partial t^\alpha}\right) = \\ &= \rho\Delta\left(\frac{\partial^\alpha p}{\partial t^\alpha}\right) + \frac{\partial\rho}{\partial x}\cdot\frac{\partial}{\partial x}\left(\frac{\partial^\alpha p}{\partial t^\alpha}\right) + \\ &+ \frac{\partial\rho}{\partial y}\cdot\frac{\partial}{\partial y}\left(\frac{\partial^\alpha p}{\partial t^\alpha}\right) + \frac{\partial\rho}{\partial z}\cdot\frac{\partial}{\partial z}\left(\frac{\partial^\alpha p}{\partial t^\alpha}\right) = \\ &= \rho\Delta\left(\frac{\partial^\alpha p}{\partial t^\alpha}\right) + \frac{\partial\rho}{\partial p}\cdot\frac{\partial p}{\partial x}\cdot\frac{\partial}{\partial x}\left(\frac{\partial^\alpha p}{\partial t^\alpha}\right) + \\ &+ \frac{\partial\rho}{\partial p}\cdot\frac{\partial p}{\partial y}\cdot\frac{\partial}{\partial y}\left(\frac{\partial^\alpha p}{\partial t^\alpha}\right) + \frac{\partial\rho}{\partial p}\cdot\frac{\partial p}{\partial z}\cdot\frac{\partial}{\partial z}\left(\frac{\partial^\alpha p}{\partial t^\alpha}\right), \end{aligned} \tag{4}$$

where Δ is the Laplace operator.

Considering that the flow in the medium is slow and the pressure gradient is of negligible significance, we neglect the last three terms in expression (4). Considering this, with constant k_f from (3) we obtain:

$$\frac{\partial(\rho m)}{\partial t} - \frac{k_f}{\mu}\rho\Delta\left(\frac{\partial^\alpha p}{\partial t^\alpha}\right) = 0. \tag{5}$$

Let's transform the first term of (5) as:

$$\frac{\partial(\rho m)}{\partial t} = m\frac{\partial \rho}{\partial t} + \rho\frac{\partial m}{\partial t} = m\frac{\partial \rho}{\partial p}\cdot\frac{\partial p}{\partial t} + \\ + \rho\frac{\partial m}{\partial p}\cdot\frac{\partial p}{\partial t} = \rho\left(m\frac{1}{\rho}\frac{\partial \rho}{\partial p} + \frac{\partial m}{\partial p}\right)\frac{\partial p}{\partial t}. \quad (6)$$

Let us take the laws of change of ρ and m with dependent to p in the form:

$$\rho = \rho_0 \cdot e^{\beta_f (p-p_0)}, \quad (7)$$

$$m = m_0 + \beta_r (p - p_0), \quad (8)$$

where ρ_0 and m_0 – are the density and porosity at $p = p_0$, p_0 – is a certain reference pressure, β_f and β_r – are the coefficients of volumetric elasticity of the liquid and the medium, respectively.

When the fluid is weakly compressible, instead of (7) we take:

$$\rho = \rho_0\left[1 + \beta_f (p - p_0)\right] \quad (9)$$

Taking into account (7), (8) from (6) we have:

$$\frac{\partial(\rho m)}{\partial t} = \rho\left(m_0\beta_f + \beta_r\right)\frac{\partial p}{\partial t}, \quad (10)$$

where in the parentheses on the right side, taking into account the smallness of the change in value, m_0 is taken instead of m.

Taking into account (10) from (5) we have:

$$\frac{\partial p}{\partial t} = \varkappa\ \Delta\left(\frac{\partial^\alpha p}{\partial t^\alpha}\right), \quad (11)$$

where $\varkappa = \dfrac{k_f}{\mu\beta^*}$ is is the coefficient of piezoconductivity, $\beta^* = m_0\beta_f + \beta_r$ is the elasticity coefficient of the medium.

For inhomogeneous media in terms of permeability, equation (11) has the form:

$$\mu\beta^*\frac{\partial p}{\partial t} = \Delta\left(k_f(x,y,z)\frac{\partial^\alpha p}{\partial t^\alpha}\right). \quad (12)$$

For homogeneous anisotropic media, the piezoconductivity equation is written as:

$$\mu\beta^*\frac{\partial p}{\partial t} = k_{fx}\frac{\partial^2}{\partial x^2}\left(\frac{\partial^\alpha p}{\partial t^\alpha}\right) + \\ + k_{fy}\frac{\partial^2}{\partial y^2}\left(\frac{\partial^\alpha p}{\partial t^\alpha}\right) + k_{fz}\frac{\partial^2}{\partial z^2}\left(\frac{\partial^\alpha p}{\partial t^\alpha}\right), \quad (13)$$

where k_{fx}, k_{fy}, k_{fz} – are the permeability coefficient in the directions, x, y, z respectively.

3 Statement of the Problem

We will consider the one-dimensional equation (11):

$$\frac{\partial p}{\partial t} = \varkappa\frac{\partial^2}{\partial x^2}\left(\frac{\partial^\alpha p}{\partial t^\alpha}\right). \quad (14)$$

For this equation it is sufficient to specify one initial and two boundary conditions, for example for a finite layer $[0, L_{med}]$:

$$p(0,x) = p_0 = const, \ , \quad (15)$$

$$p(t,0) = p_c = const\ , p(t, L_{med}) = 0\ . \quad (16)$$

In addition to (16), let us consider the following regime of pressure change at the boundaries:

$$p(t,0) = p_c\left(1 - \exp\left(-\omega\cdot t\right)\right),\ p(t, L_{med}) = 0,$$

$$\omega = const. \quad (17)$$

$$p(t,0) = p_c\left(1 + \sin\left(\omega\cdot t\right)\right),\ p(t, L_{med}) = 0\ . \quad (18)$$

4 Numerical Solution Algorithm

Equation (14) under conditions (15) – (18) is solved by the finite difference method, [14], [15], [16], [17], [18]. To do this, we introduce a grids $\overline{\omega}_h = \{x_i = i\cdot h,\ i = 0,2,\ldots N\}$, $\overline{\omega}_\tau = \{t_j = j\cdot\tau,\ j = 0,1,2,\ldots T\}$ in the region $\{0 \le t \le T_{\max},\ 0 \le x \le L_{med}\}$ where h is the grid step in the direction x, τ is the grid step in time. From these two grids, we construct two-dimensional meshes $\overline{\omega} = \overline{\omega}_h \times \overline{\omega}_\tau$. Its nodes consist of $(x_i, t_j),\ i = \overline{0,N};\ j = 0,1,2,\ldots$ points.

On this grid, equation (14) is approximated as [19], [20], [21], [22]:

$$p_i^{j+1} - p_i^j = \varkappa\frac{1}{\Gamma(2-\alpha)h^2\tau^\alpha}\cdot\left[\left(\sum_{k=0}^{j-1}(p_{i+1}^{k+1} - p_{i+1}^k)\cdot\right.\right. \\ \cdot\left((j-k+1)^{1-\alpha} - (j-k)^{1-\alpha}\right) + p_{i+1}^{j+1} - p_{i+1}^j\Big) - \\ - 2\cdot\left(\sum_{k=0}^{j-1}(p_i^{k+1} - p_i^k)\cdot\left((j-k+1)^{1-\alpha} - (j-k)^{1-\alpha}\right) + \right. \\ + p_i^{j+1} - p_i^j\Big) + \left(\sum_{k=0}^{j-1}(p_{i-1}^{k+1} - p_{i-1}^k)\cdot\right. \\ \left.\left.\cdot\left((j-k+1)^{1-\alpha} - (j-k)^{1-\alpha}\right) + p_{i-1}^{j+1} - p_{i-1}^j\Big)\right] \quad (19)$$

$i = \overline{1,N}\ ;\ j = \overline{0,T_{\max}}\ ;\ k = \overline{0,j}\ .$

We introduce the following notations:

$$S_{P1}=\sum_{k=0}^{j-1}\left(p_{i+1}^{k+1}-p_{i+1}^{k}\right)\cdot\left((j-k+1)^{1-\alpha}-(j-k)^{1-\alpha}\right), \quad (20)$$

$$S_{P2}=\sum_{k=0}^{j-1}\left(p_{i}^{k+1}-p_{i}^{k}\right)\cdot\left((j-k+1)^{1-\alpha}-(j-k)^{1-\alpha}\right), \quad (21)$$

$$S_{P3}=\sum_{k=0}^{j-1}\left(p_{i-1}^{k+1}-p_{i-1}^{k}\right)\cdot\left((j-k+1)^{1-\alpha}-(j-k)^{1-\alpha}\right), \quad (22)$$

$$k_p=\varkappa\,\frac{\tau^{1-\alpha}}{\Gamma(2-\alpha)h^2}. \quad (23)$$

Substituting the above notations into equation (19), we obtain:

$$\begin{aligned}p_i^{j+1}-p_i^j=k_p\left(S_{p1}+p_{i+1}^{j+1}-p_{i+1}^j\right)-\\-2k_p\left(S_{p2}+p_i^{j+1}-p_i^j\right)+k_p\left(S_{p3}+p_{i-1}^{j+1}-p_{i-1}^j\right).\end{aligned} \quad (24)$$

Equation (24) takes the following form

$$Ap_{i+1}^{j+1}-Bp_i^{j+1}+Cp_{i-1}^{j+1}=-F_i^j, \quad (25)$$

where $A=k_p;\ B=2k_p+1;\ C=k_p;$

$$F_i^j=\left(p_i^j-k_p\left(2p_i^j-p_{i+1}^j+S_{p1}-2S_{p2}+S_{p3}-p_{i-1}^j\right)\right).$$

The system of equations (25) is solved by the sweep method.

The initial condition is approximated as $p_i^0=p_0$,

$$i=\overline{0,N}. \quad (26)$$

Boundary conditions (16) – (18) in difference form have the form:

$$\text{a)}\ p_0^{j+1}=p_c,\ p_N^{j+1}=0,\ j=0,1,... \quad (27)$$

$$\text{b)}\ p_0^{j+1}=p_c\left(1-e^{-\omega(j+1)\tau}\right),\ p_N^{j+1}=0,\ j=0,1,... \quad (28)$$

$$\text{c)}\ p_0^{j+1}=p_c\left(1+\sin\left(\omega\left(j+1\right)\tau\right)\right),\ p_N^{j+1}=0,\ j=0,1,.... \quad (29)$$

The system of equations (25) is solved by the Thomas' algorithm. We use the following relationship:

$$p_i^{j+1}=\delta_{i+1}\cdot p_{i+1}^{j+1}+\eta_{i+1}. \quad (30)$$

where δ_{i+1}, η_{i+1} are coefficients of Tomas algorithm.

Using (30) from (25) we obtain the following recurrence formulas for determining the coefficients δ_{i+1}, η_{i+1}

$$\delta_{i+1}=\frac{-C}{A\cdot\alpha_i-B},\ \eta_{i+1}=\frac{-\left(F+A\cdot\beta_i\right)}{A\cdot\alpha_i-B}. \quad (31)$$

The initial values of the coefficients δ_{i+1}, η_{i+1} are determined based on conditions (27)–(29): $\eta_1=p_c$, $\delta_1=0$.

Note that sufficient stability conditions for apply Thomas' algorithm to equations (25) are satisfied.

5 Discussion and Results

Some of the computational results are shown in Figure 1, Figure 2, Figure 3, Figure 4, Figure 5, Figure 6, Figure 7, Figure 8, Figure 9, Figure 10, Figure 11 and Figure 12 for different model parameters. The following parameter values are used: $k_f=10^{-13}\,\mathrm{m}^2\cdot\mathrm{s}^{\alpha}$, $\mu=10^{-2}\,Pa\cdot s$, $\beta^*=10^{-10}\,Pa^{-1}$, $p_c=5\cdot10^5\,Pa$, $p_0=0$, $L_{med}=30\ m$. The following grid parameters were used: $h=0.1$, $\tau=1$.

Initially given results for the boundary condition (3.3).

Figure 1 shows the dynamics of the evolution of the pressure distribution in the medium at different moments of time for some values of the parameter α. The evolution of its profiles with increasing time can be detected from the pressure distribution. For large times, a stationary pressure distribution over the medium is established, which is a straight line from $p(t,0)=p_0$ to $p(t,L_{med})=0$. At $\alpha=0$, i.e., in the classical case in the absence of memory effects (Figure 1a), such a distribution is practically achieved at $t=3600\ s$. With increasing the values of α Figure 1b:, Figure 1c:, Figure 1d:, at the same values of time, can be noticed a lag in the evolution of the pressure distribution in the medium. At the same time, for the larger α, this lag is stronger. While at $t=3600\ s$ in the classical case with $\alpha=0$ Figure 1a the stationary pressure distribution is almost reached, at $\alpha=0.2;\ 0.4;\ 0.6$ (Figure 1b, 1c, 1d) the pressure distribution is far from the stationary state.

In order to more clearly show the change in pressure distribution with increasing the α, the distributions of p at fixed time are shown separately Figure 2. At each values of time, a lag in the pressure distribution can be observed as α increases. At the same time, the larger the value of α, the stronger the lag. Over time, the progression of profiles in the environment can be observed.

For the cases analyzed above, the distributions of filtration velocity in the medium were constructed, which are shown in Figure 3 and Figure Figure 4. Similar to pressure, there is a decrease in the distribution of filtration velocity υ with

increasing the value of α Figure 3. So the maximum value of υ at $x=0$ is $\sim 3\cdot 10^{-7}\ (\alpha=0)$, $\sim 1.2\cdot 10^{-7}\ (\alpha=0.2)$; $0.45\cdot 10^{-7}\ (\alpha=0.4)$; $\sim 0.145\cdot 10^{-7}\ (\alpha=0.6)\ \frac{m}{s}$ at time $t=900\ s$. As time increases, these values decrease further. At $t=3600\ s$ when $\alpha=0$ (the classical case), a constant filtration velocity is practically obtained, which corresponds to a constant pressure gradient. For $\alpha=0.2;0.4;0.6$, this regime is not reached at $t=3600\ s$. In contrast to the pressure distribution, the decreasing velocity of υ is various in different values of x. The velocity υ decreases with increasing t at small values of x and increases at certain x with increasing t. Curves υ at higher t intersect curves at lower t, etc. at the points of intersection the filtration velocity outpaces the values achieved at lower t. Such intersection points with increasing α have smaller coordinates x. This is due to the lagging development of profiles υ. Based on Figure 3, we present the coordinates x, when the filtration velocity regime changes from smaller to larger with increasing time at different values of α Table 1.

Table 1. coordinates x, when the filtration velocity regime changes

t, s	t, s		
	1800	2700	3600
	$\alpha=0$		
900	14	14.2	14.5
1800		14.6	15
3600			15.2
	$\alpha=0,2$		
900	10.5	11	12
1800		12.5	13
3600			15
	$\alpha=0,4$		
900	7	7.8	8
2700		8.4	9
3600			9.6
	$\alpha=0,6$		
900	4.8	5.2	5.7
2700		5.9	6.4
3600			6.9

Source: created by the authors

As can be seen from Table 1, the coordinates when filtration velocity regime changes decreases in the increasing values of α.

The filtration velocity profiles for two values of t at increasing α are shown in Figure 4. From the graphs presented, it is clearly seen that values of υ decreases with increasing the values of α.

The obtained data confirm the conclusions of [8] that the filtration law (1) characterizes the memory effects associated with a decrease in the permeability of the medium. Here, the pseudo-permeability coefficient k_f is taken as a constant value. The decrease of the total conductivity of the medium is controlled by parameter α.

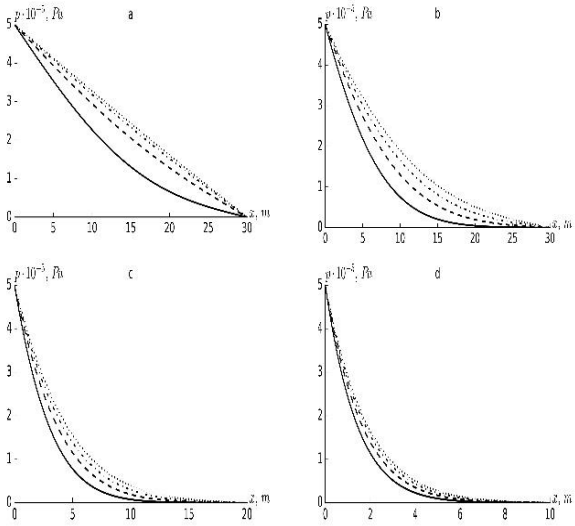

Fig. 1: Pressure profiles at $\alpha=0\ (a)$, $0.2\ (b)$, $0.4\ (c)$, $0.6\ (d)$, $t=900$ (——), 1800 (- - -), $2700\ (-\cdot-\cdot-)$, $3600\ (\cdots\cdots)$

Source: created by the authors

Very small values of υ Figure 3 are explained by the compressibility of the fluid and the skeleton of the porous medium, since the elastic filtration mode is considered. The pressure forces are used to do the work of compressing the fluid and the skeleton of the porous medium.

Similar calculations were performed with boundary conditions (17). The first condition (17) corresponds to exponential pressure growth at the boundary $x=0$ from 0 to p_c. Depending on the size of the $\emptyset$, this growth can have different velocities. Some results of pressure variation at different time points for different values of α are shown in Figure 5. In contrast to the previous case $p(t,0)=p_c$, in the present case at $x=0$ the pressure increases gradually in time, resulting in a relatively slow advanced of pressure profiles throughout the medium. The parameter α leads to slower advanced of profiles of p.

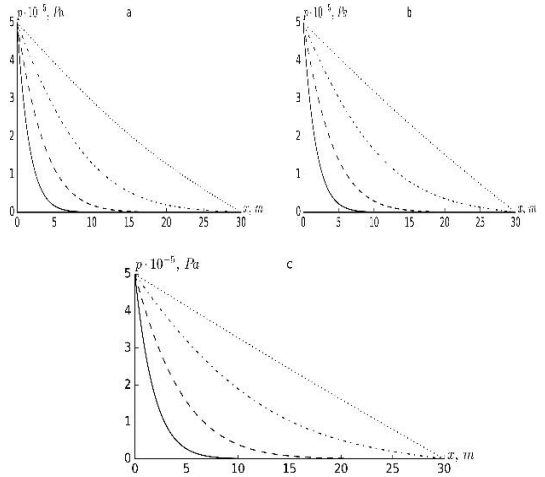

Fig. 2: Pressure profiles for different α at $t=1800$ (a), 2700 (b), 3600 (c) s, $\alpha=0$ $(\cdots\cdots)$, 0.2 $(-\cdot-\cdot-)$, 0.4 (- - - -), 0.6 (——)

Source: created by the authors

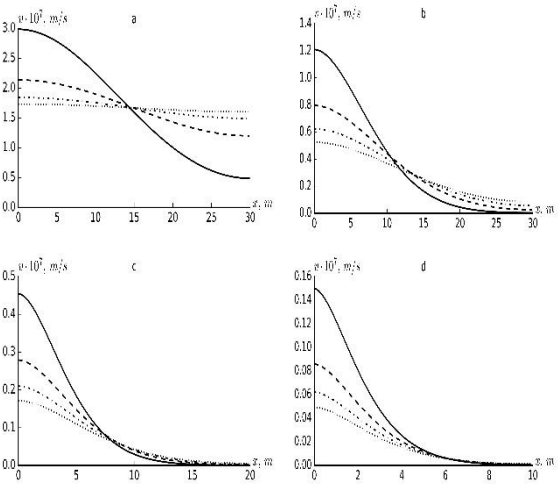

Fig. 3: Profiles of filtration velocity $\alpha=0$ (a), 0.2 (b), 0.4 (c), 0.6 (d), $t=900$ (——), 1800 (- - -), 2700 $(-\cdot-\cdot-)$, 3600 $(\cdots\cdots)$s

Source: created by the authors

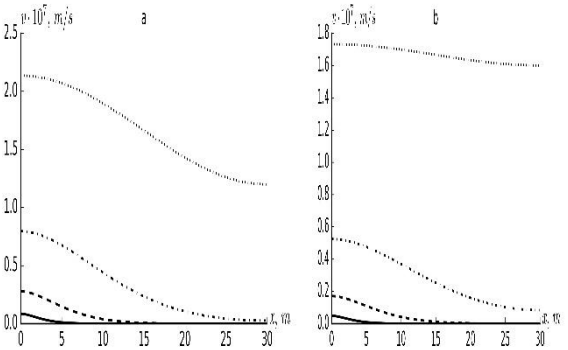

Fig. 4: Profiles of filtration velocity different α at $t=1800$ (a), 3600 (b) s, $\alpha=0$ $(\cdots\cdots)$, 0.2 $(-\cdot-\cdot-)$, 0.4 (- - - -), 0.6 (——)

Source: created by the authors

Thus, the boundary condition (17) and the increase in value of α act in the same way, both slowing down the advanced of pressure profiles. Due to slow growth of the boundary pressure (at $x=0$), the onset of the static regime is also slowed down. This can be verified by comparing Figure 1a: and Figure 5a. To see more clearly the effect of α on advanced of p its graphs are plotted for different values of α at some points of time Figure 6. As can be seen from the figures, increasing values of α leads to slower advanced of p. As t increases, the graphs spread in the environment. For all considered values of α and given times $t=1800$, 2700 , 3600 s the stationary regime is not reached.

On the basis of pressure profiles Figure 5, Figure 6 the filtration velocity fields are plotted in Figure 7, Figure 8. The character of filtration velocity change remains the same as in the case of constant boundary pressure Figure 3, Figure 4. The difference is a decrease in the values of υ at the corresponding points of x for the same values of α and t. This is due to the slowing down of the pressure growth velocity at the boundary $x=0$ and, consequently, of the pressure gradient in the medium. As in the case of pressure changes, the growth of α and the gradual increase in pressure at the $x=0$ boundary additively slows the development of filtration velocity profiles.

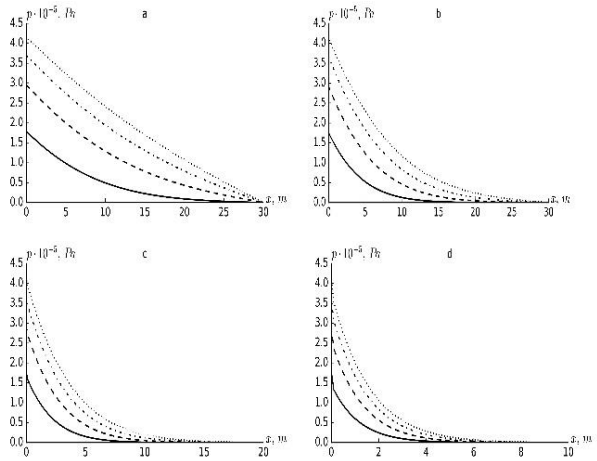

Fig. 5: Pressure profiles at $\alpha=0$ (a), 0.2 (b), 0.4 (c), 0.6 (d), $t=900$ (——), 1800 (- - -), 2700 $(-\cdot-\cdot-)$, 3600 $(\cdots\cdots)$ s

Source: created by the authors

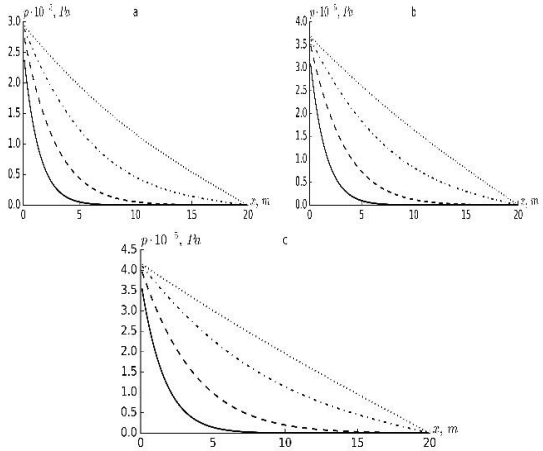

Fig. 6: Pressure profiles for different α at $t=1800$ (a), 2700 (b), 3600 (c) s, $\alpha=0$ $(\cdots\cdots)$, 0.2 $(-\cdot-\cdot-)$, 0.4 (- - - -), 0.6 (——)

Source: created by the authors

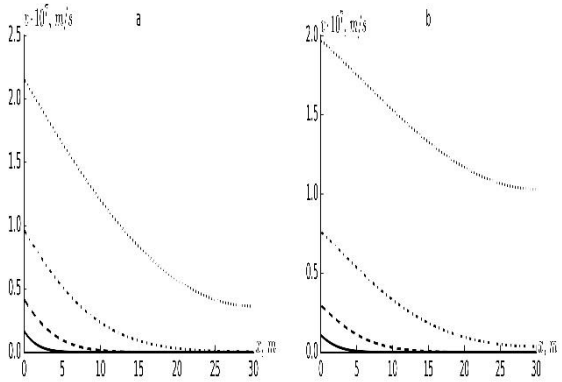

Fig. 7: Profiles of filtration velocity at $\alpha=0\,(a)$, $0.2\,(b)$, $0.4\,(c)$, $0.6\,(d)$, $t=900$ (——), 1800 (- - -), 2700 $(-\cdot-\cdot-)$, 3600 $(\cdots\cdots)$s

Source: created by the authors

Now let us consider the results obtained for the boundary conditions (18). In this case, the pressure at the boundary $x=0$ varies according to a sinusoidal law. The variation of p at different time points of t for some values of α is shown in Figure 9. In contrast to the previous cases, in this case we obtain a non-monotonic change of pressure in the medium with increasing time t.

In the phase of pressure increase at the boundary, when $0\le\omega t\le\frac{\pi}{2}$, the pressure in the medium increases. In the depressurization phase at the boundary, when $\frac{\pi}{2}\le\omega t\le\frac{3\pi}{2}$, the pressure in the medium starts to decrease starting from the boundary $x=0$. At $t=600\ s$, the pressure up to point A Figure 9a will be lower than the pressure at $t=300\ s$. At time $t=900\ s$, the pressure up to point B will be lower than the pressure at $t=300\ s$.

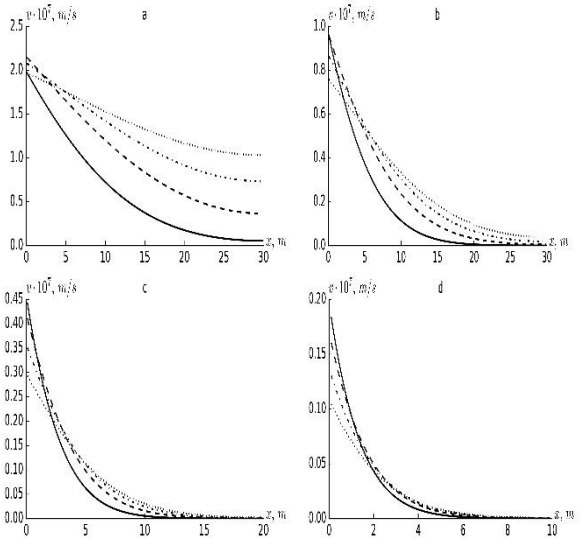

Fig. 8: Profiles of filtration velocity different α at $t=1800$ (a), 3600 (b) s, $\alpha=0$ $(\cdots\cdots)$, 0.2 $(-\cdot-\cdot-)$, 0.4 (- - - -), 0.6 (——)

Source: created by the authors

At $t=1200\ s$, the area of reduced pressure compared to $t=300\ s$ reaches the C point. At $t=1500\ s$, when the boundary pressure reaches ~ $2p_c$, a pressure higher than at $t=300\ s$ is established in the entire medium region. When $\frac{5\pi}{2}\le\omega t\le3\pi$, the pressure at the boundary $x=0$ decreases and this causes the pressure in the medium to decrease starting at $x=0$. The pressure graph at $t=1800\ c$ intersects the graph at $t=300\ s$ at point D, which have coordinate less than the coordinate of point A. This is explained by the fact that in the first cycle of pressure change during the period $0\le\omega t\le2\pi$, the pressure in the medium developed from the initial zero state according to the initial condition $p(0,x)=p_0=0$. At $\frac{5\pi}{2}\le\omega t\le3\pi$, the pressure change starts from the state of the pressure distribution at $\omega t=\frac{5\pi}{2}$, which is naturally non-zero. This also explains why the pressure distribution is everywhere higher at $t=1500\,s$ than the distribution at $t=300\,s$. Thus, the harmonic mode of pressure variation at the boundary $x=0$ leads to oscillatory pressure variation up to certain distances from the boundary. Comparing the plots of Figure 9, we can observe a decreasing of p

development with increasing the values of α. The delaying effect of α can also be seen in the plots of Figure 10a, Figure 10b which show the pressure distribution at different values of α for two time points. As the α value increases, there is clearly a delay in the development of pressure profiles.

The change in filtration velocity corresponding to the parameter change options in Figure 9a, Figure 11b is shown in Figure 11a, Figure 12b. The most distinctive feature of change of υ in this case is the appearance of its negative values, etc. the presence of reverse filtration flows. This is a consequence of the non-monotonic pressure distribution in the medium. In the depressurization regime, the pressure at the $x=0$ boundary within the medium has a higher value than at other values of x. In the zone where p has an increasing distribution the pressure gradient has positive values, which according to Darcy's law gives a negative value of υ. A reverse flow occurs in this area. At the same time, in the zone of pressure decrease along x, filtration flow towards the $x=L_{med}$ end continues. Thus, from the point with maximum value of p inside the medium, filtration flow develops both to the right and to the left.

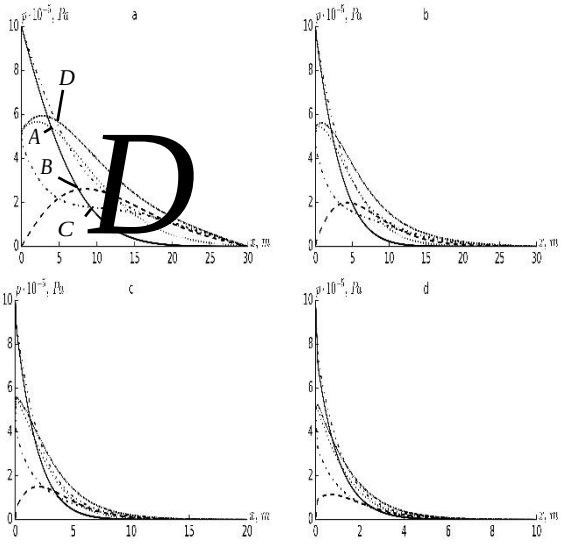

Fig. 9: Pressure profiles at $\alpha=0\,(a)$, $0.2\,(b)$, $0.4\,(c)$, $0.6\,(d)$, $t=300$ (——), 600 $(\cdots\cdots)$, 900 (- - -), 1200 $(-\cdot-\cdot-)$, 1500 $(-\cdot\ \cdot-\cdot\ \cdot-)$, 1800 $(-\cdot\cdot-\cdot\cdot-)$s

Source: created by the authors

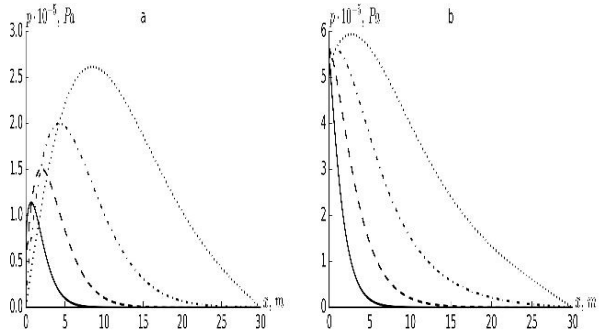

Fig. 10: Pressure profiles for different α at $t=900$ (a), 1800(b) s, $\alpha=0$ $(\cdots\cdots)$, 0.2 $(-\cdot-\cdot-)$, 0.4 (- - -), 0.6 (——)

Source: created by the authors

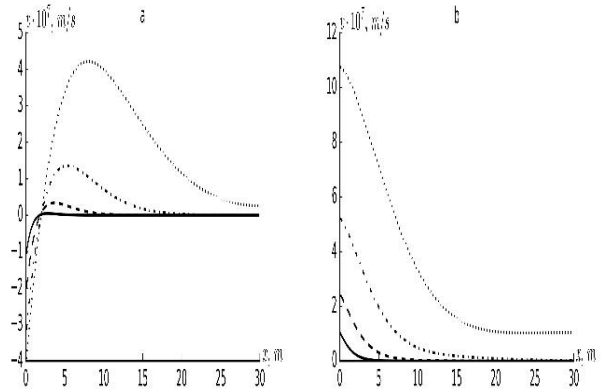

Fig. 11: Profiles of filtration velocity at $\alpha=0\,(a)$, $0.2\,(b)$, $0.4\,(c)$, $0.6\,(d)$, $t=300$ (——),600 $(\cdots\cdots)$, 900 (- - -), 1200 $(-\cdot-\cdot-)$, 1500 $(-\cdot\ \cdot-)$, 1800 $(-\cdot\cdot-\cdot\cdot)$ s

Source: created by the authors

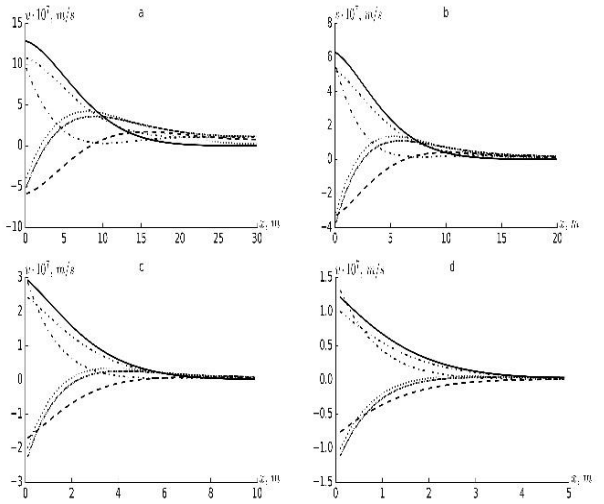

Fig. 12: Profiles of filtration velocity different α at $t=1800$ (a), 3600 (b) s, $\alpha=0$ $(\cdots\cdots)$, 0.2 $(-\cdot-\cdot-)$, 0.4 (- - - -), 0.6 (——)

Source: created by the authors

As values of α increases, values of υ decreases and the zone of distribution of filtration velocity in the medium decreases. This means that the zone of fluid flow does not reach the end of the $x = L_{med}$.

In Figure 11b, Figure 11c, Figure 11d it can be found that υ reaches almost zero values with increasing values of α at relatively small values of x. This can also be verified from the pressure distribution shown in Figure 9b, Figure 9c, Figure 9d. They show how, with the increasing the value of α, a zone with almost zero pressure gradient appears starting at which x. For two values of time t, the distribution of υ with increasing values of α is shown. The delaying effect of α on the development of υ is clearly visible in the graphs.

6 Conclusions

The piezoconductivity equation based on the generalized Darcy's law is supplemented with a fractional derivative of the pressure gradient, which allows more accurate modeling of filtration processes in porous media with delays and memory effects. The introduction of the fractional derivative reflects more complex processes that cannot be described by traditional differential operators. This leads to slower changes in pressure and filtration velocity, especially since significant delay effects were observed when the order of the fractional derivative was increased. This means that the higher the order of the fractional derivative, the more pronounced the delay effects on the pressure variance and filtration velocity. When the ambient boundary pressure is given in exponential form, there is a more pronounced lag of pressure profiles and filtration velocities. When the pressure at the boundary of the environment is varied in a sinusoidal mode, non-monotonicity of the pressure and filtration velocity distributions is observed. In particular, up to a certain distance from the boundary of the medium, oscillatory changes in pressure and velocity profiles appear, which indicate the phenomena of inertial shock in porous medium. An important part of this process is the formation of reverse filtration currents. This behavior indicates that filtration in the medium can occur in the direction opposite to the direction of the initial pressure. These results show that the fractional derivative of Darcy's law can account for memory effects, which is important for modeling filtration in complex, porous, or anisotropic media such as oil reservoirs or groundwater.

Declaration of Generative AI and AI-assisted Technologies in the Writing Process

The authors wrote, reviewed and edited the content as needed and verifies that none utilized artificial intelligence (AI) tools were used. The authors take full responsibility for the content of the publication.

References:

[1] Caputo M, Models of flux in porous media with memory, *Water Resources Research*, Vol.36, No.3, 2000, pp.693–705, doi.org/10.1029/1999WR900299.

[2] Obembe A.D & Hossain M.E & Mustapha K & Abu - Khamsin S.A, A modified memory-based mathematical model describing fluid flow in porous media, *Computers and Mathematics with Applications*, Vol.73, No.6, 2017, pp. 1385-1402, https://doi.org/10.1016/j.camwa.2016.11.022.

[3] Chang A & Sun H & Zhang Y & Zheng C & Min F, Spatial fractional Darcy's law to quantify fluid flow in natural reservoirs, *Physica A*, Vol.519, 2019, pp.119-126, https://doi.org/10.1016/j.physa.2018.11.040.

[4] Di Giuseppe E & Moroni M & Caputo M, Flux in porous media with memory: models and experiments, *Transport in Porous Media*, Vol.83, 2010, pp.479-500, doi: 10.1007/s11242-009-9456-4.

[5] Plastino W & Caputo M, Diffusion in porous layers with memory, *Geophysical Journal International*, Vol.158, No.1, 2004, pp.385-396, https://doi.org/10.1111/j.1365-246X.2004.02290.x.

[6] Shaw S & Seikh A, Higher Order Generalized Thermoelastic Model with Memory Responses in Nonhomogeneous Elastic Medium due to Laser Pulse. *WSEAS Transactions on Applied and Theoretical Mechanics*, Vol.*19*, No.3, 2024, pp.2135. https://doi.org/10.37394/232011.2024.19.3.

[7] Caputo M, Diffusion with space memory modeled with distributed order space fractional differential equations, *Annals of Geophysics*, Vol.46, No.2, 2003, pp.223-234, https://doi.org/10.4401/ag-3395.

[8] Erika Di Giuseppe & Monica Moroni & Michele Caputo, Flux in porous media with memory: models and experiments, *Transport in Porous Media*, Vol.83, 2010, pp.479-500 doi: 10.1007/s11242-009-9456-4.

[9] Caputo M. Diffusion of fluids in porous media with memory, *Geothermics*, Vol.28, No.1, 1999, pp.113-130,

https://doi.org/10.1016/S0375-6505(98)00047-9.

[10] Hossain M.E & Liu L & Islam M.R, Inclusion of the memory function in describing the flow of shear-thinning fluids in porous media, *International Journal of Engineering (IJE)*, Vol.3, No.5, 2009, pp.458-478.

[11] M.E. Hossain & S.H. Mousavizadegan & C. Ketata & M.R. Islam, "A Novel Memory Based Stress-Strain Model for Reservoir Characterization". *Journal of Nature Science and Sustainable Technology*, Vol.1, No.4, 2007, pp.653-678.

[12] Basniev K.S &Vlasov A.M & Kochina I.N. & Maksimov V.M, *Underground hydraulics* - M.: Nedra, 1986.

[13] Aziz K & Settari A, *Petroleum reservoir simulation.* Applied science publishers LTD.London. 1979.

[14] Samarsky A.A, *Theory of difference schemes*, – M.: Nauka, 1989.

[15] Xiao-jun Yang, *General Fractional Derivatives. Theory, Methods and Applications*, Taylor Francis Group: LLC, 2019. https://doi.org/10.1201/9780429284083.

[16] Khuzhayorov B & Usmonov A & Nik Long N.M.A & Fayziev B, Anomalous solute transport in a cylindrical two-zone medium with fractal structure, *Applied Sciences (Switzerland),* Vol.10, No.15, 2020, doi: 10.3390/app10155349.

[17] Khuzhayorov B.K & Dzhiyanov T.O & Mamatov S.S & Shukurov V.S, Mathematical model of substance transport in two-zone porous media, *In AIP Conference Proceedings*, Vol.2637, No.1, 2022, https://doi.org/10.1063/5.0118450.

[18] Alikhanov A.A, Numerical methods of solutions of boundary value problems for the multi-term variable-distributed order diffusion equation, *Applied Mathematics and Computation*, Vol.268, 2015.

[19] Dzhiyanov T.O & Mamatov S & Zokirov M.S, Anomalous Solute Transport in an Inhomogeneous Porous Medium Taking into Account Mass Transfer, *International Conference on Actual Problems of Applied Mathematics and Computer Science. – Cham: Springer Nature Switzerland*, 2022, pp.45-53, doi: 10.1007/978-3-031-34127-4_5.

[20] Lu X,Z & Liu F.W, Time fractional Diffusion-Reaction equation, *Numerical Mathematics A Journal of Chinese Universities.* Vol.27, No.3, 2005, pp.267-273.

[21] Makhmudov J.M & Usmonov A.I & Kuljonov J.B, Solution of the Anomalous Filtration Problem in Two Dimensional Porous Media, *APAMCS, LNNS*, Vol.702, 2022, pp.68–80, doi: 10.1007/978-3-031-34127-4_7.

[22] Makhmudov J.M & Usmonov A.I & Kaytarov Z.D & Sultonov B, Numerical solution of the problem of anomalous solute transport in a two-dimensional nonhomogeneous porous medium, *AIP Conference Proceedings*, Vol.2637, No.1, 2022, https://doi.org/10.1063/5.0118488.

Contribution of Individual Authors to the Creation of a Scientific Article (Ghostwriting Policy)

Khuzhayorov B has derived the mathematical model and interpreted the results.
Dzhiyanov T. approximated the model.
The results were obtained in Python using the model and its approximation, and the overall framework was structured by Sh. Akramov.

Sources of Funding for Research Presented in a Scientific Article or Scientific Article Itself

No funding was received for conducting this study.

Conflict of Interest

The authors declare that there is no conflict of interest.